

## HYDRODYNAMICS OF ISOTHERMAL UPWARD TWO PHASE FLOWS IN HELICAL COILS

Mahmood Reza Rahimi<sup>1</sup>, Aboalfazl Askari<sup>1</sup>, Mehdi Ghanbari<sup>1,2</sup>

<sup>1</sup>*Process Intensification Lab., Chemical Engineering Department, School of Engineering, Yasouj University, Yasouj 75918-74831, Iran;* <sup>2</sup>*Department of Petroleum and Chemical Engineering, Shiraz University, Shiraz, Iran.*

Received August 8, 2014, Accepted October 10, 2014

---

### Abstract

The hydrodynamic characteristics of isothermal upward turbulent two-phase flow of dispersed air-water in helical coils were investigated using computational fluid dynamics. Population Balance Modeling (PBM) approach was applied for size distribution of poly-dispersed air produced by coalescence and breakup of bubble groups. The main aim of this work is to examine the ability of proposed coupled CFD-PBM model, especially to show hydrodynamic characteristics as well as the influence of  $k-\epsilon$  and Shear Stress Transport (SST) turbulence models on performance of CFD-PBM model. The detailed analysis of the flow in helical coils has been carried out using velocity, pressure, air volume fraction and secondary flow. The weakness of  $k-\epsilon$ -CFD-PBM combined model is revealed in comparison to the SST-CFD-PBM combined model. In addition, the significance of replacing the helical pipes instead of directed-line pipes was briefly studied. It is found that the orientation of the dispersed phase in two phase flow through the kinds of bent tubes such as helical pipe and U-tubes maybe controls their applicabilites in heat exchanger tools.

**Keywords:** helical coils; two phase flow; poly-dispersed flow; CFD; shear stress transport model.

---

### 1. Introduction

Helically coiled heat exchangers have obtained very wide range of industrial applications such as, nuclear industry, steam generators, heat recovery systems, etc. [1-2]. This is due to the unique hydraulic and thermal characteristics of helical coils in comparison to the straight-line tubes.

The study on hydraulic and thermal properties of helical coils is useful because of the fact that the results of such studies can be expanded to other similar geometry of instruments. For example, these studies may be easily extended to deal with a bent tube [3] embedded in a heat exchanger or a non-zero pitch bend tube in a riser tube of a high-pressure boiler. In many cases, the fluid which is flowing through the helical coil, is in the form of two-phase flow. The orientation of the dispersed phase in two-phase flow through the kinds of bent tubes such as helical coil and U-tubes may controls the unexpected failure occurred in heat exchanger tools. The report of unexpected failures of tubes through which two-phase flow is streamed is published in detail [4].

Although the results of studies on two-phase flow in straight pipes are widely reported [5-6], for helical and U-tubes, the results are not widely available. Kasturi and Stepanek [7], among others, carried out pressure drop and void fraction measurements for gas-liquid two-phase counter-flow in a helical coil. Czop *et al.* (1994) [8] carried out experiments on water-SF<sub>6</sub> flow through a helically coiled tube of 19.8mm pipe diameter with 1170mm coil diameter.

Several authors have proposed different models to describe the bubble coalescence and breakup processes [9-10]. Instead of arbitrarily considering two bubble classes, it may be useful to incorporate a coalescence and break-up model based on the Multiple Size Group (MUSIG) model framework in the Computational Fluid Dynamic (CFD) model. Jayakumar *et al.* [11] have studied the characteristics of two-phase flow in helical coils using two-fluid Eulerian-

Eulerian scheme. In the later study the diameter of the bubbles had been kept constant ( $d = 0.1$  mm). Although they carried out an intensive work, showing the contour plots of velocity, temperature and air volume fraction, their results have a degree of ambiguities and in some cases, it seems that are not physical meaningful (especially regarding their air volume fraction contour plots). Starting the investigations of the single phase water flow in U-tubes using Shear Stress Transport (SST) model and Explicit Algebraic Reynolds Stress Model (EARSM), good agreement between Computational Fluid Dynamics (CFD) solution and experimental data provided by Takamasa and Kondo [12].

In the case of two-phase flow in helical coils, no such publication of poly-dispersed phase is available. On the other hand, the role of turbulence models on the performance of CFD-PBM model to capture the behavior of two-phase flow in helical coils is very important. So, the main aim of this work is to study different modeling schemes, including combination of two turbulence models coupled with the bubble size distribution model.

## 2. Modeling

### 2.1 Multiple Size Group (MUSIG) Model

By interaction of the bubbles with each other through the mechanisms of breakup and coalescence, a poly-dispersed phase is developed. The population balance model by providing a mathematical definition for bubble size distribution is an effective technique for the modeling of poly-dispersed phase. MUSIG model is a framework that incorporates the population balance equation into CFD calculations.

### 2.2 Population Balance Equation

The bubble size distribution plays an important role in the flow patterns and hydrodynamic behaviours of the two-phase flows. The accurate determination of the bubble size distribution can significantly affect the accuracy of hydrodynamics calculations fluid flow field. The spatial distribution of void fraction and velocities of both phases may be influenced by bubble size distribution. These influences can be taken into account in computational fluid dynamics (CFD) simulations.

The governing equations without interface heat and mass transfer, in the Eulerian-Eulerian scheme can be written as follows. There is the liquid phase as continuous phase and the dispersed gas phase as discrete bubble sizes tracked by solving an additional set of transport equations. These equations are progressively coupled with the flow equations during the simulation.

Continuity equation (liquid phase):

$$\frac{\partial}{\partial t}(\rho_l \alpha_l) + \nabla \cdot (\rho_l \alpha_l \mathbf{u}_l) = 0 \quad (1)$$

Continuity equation (gas phase):

$$\frac{\partial}{\partial t}(\rho_g \alpha_g f_i) + \nabla \cdot (\rho_g \alpha_g \mathbf{u}_g f_i) = P_i^B + P_i^C - D_i^B - D_i^C \quad (2)$$

where  $\rho$  is the mass density,  $\alpha$  is the volume fraction,  $\mathbf{u}$  is the volume averaged velocity,  $f$  is the volume fraction of bubbles.

The right hand side of Eq .2 represents a source term that is the algebraic sum of the death and birth of bubbles caused by coalescence and breakup processes. The production rates due to coalescence and breakup of bubbles is represented as:

$$P_i^C = \frac{1}{2} \sum_{k=1}^N \sum_{l=1}^n \chi_{i,kl} n_k n_l \quad (3a)$$

$$P_i^B = \sum_{j=1}^n \Omega(V_j : V_i) n_j \quad (3b)$$

and the death rate due to coalescence and breakup of bubbles are

$$D_i^C = \sum_{j=1}^n \chi_{ij} n_i n_j \quad (4c) \quad D_i^B = \Omega_i n_i \quad (4)$$

P is the production rate, D is the consumption rate, n is the bubble number density, V is the volume of a bubble.

The relation between the bubble number density and gas volume fraction is given by:

$$\alpha_g f_i = n_i V_i \quad (5)$$

The breakup of bubbles in turbulent dispersions is represented by the model developed by Luo and Svendsen [10] and the coalescence rate resulted from turbulent collision is taken into account by Prince and Blanch model [9].

The momentum conservation for liquid and gas phase is as follows:

$$\frac{\partial}{\partial t}(\rho_l \alpha_l u_l) + \nabla \cdot (\rho_l \alpha_l u_l u_l) = -\alpha_l \nabla p + \rho_l \alpha_l g - \nabla(\tau_l \alpha_l) + F_D \quad (6)$$

$$\frac{\partial}{\partial t}(\rho_g \alpha_g u_g) + \nabla \cdot (\rho_g \alpha_g u_g u_g) = -\alpha_g \nabla p + \rho_g \alpha_g g - \nabla(\tau_g \alpha_g) - F_D \quad (7)$$

The  $F_D$  in Eqs. 6 and 7 represents Drag force.

$$F_D = \frac{3}{4} C_D \alpha_g \rho_l \frac{1}{d_b} |u_l - u_g| (u_l - u_g) \quad (8)$$

For the distorted bubbles, the drag coefficient is affected by the particle shape through the dimensionless group known as the Eotvos number ( $Eo$ ). The Ishii-Zuber correlation for drag coefficient gives [13]:

$$C_D = \frac{2}{3} Eo^{0.5} \quad (a) \quad (9)$$

$$Eo = \frac{g(\rho_l - \rho_g)d_p^2}{\sigma} \quad (b)$$

Here,  $d$  and  $\delta$  are the diameter and the surface tension, respectively, and  $Eo$  is the Eotvos number.

The size groups have been set using equal diameter discretization. In all cases, the diameter and mass of a particular group are related by:

$$m = \frac{\pi}{6} \rho_d d^3 \quad (10)$$

In the case of equal diameter discretization, the diameter of group  $i$  is calculated from:

$$d_i = d_{min} + \Delta d \left( i - \frac{1}{2} \right) \quad (11)$$

$$\Delta d = \frac{d_{max} - d_{min}}{N} \quad (12)$$

### 3. Turbulence Models

#### 3.1. k-ε model

The presence of wakes behind the large dispersed particles resulted in an increase in turbulence in the continuous phase. This is known as particle (bubble) induced turbulence. The Sato Enhanced Eddy Viscosity model is used to model that [14]. The k-ε single phase (continuous phase) turbulence model can be extended to poly-dispersed model by incorporating the Sato's bubble-induced turbulent viscosity model. The governing equations for the turbulent kinetic energy,  $k$  and turbulent dissipation,  $\varepsilon$  are:

$$\frac{\partial}{\partial t}(\rho_l \alpha_l k) + \nabla \cdot \left[ \alpha_l \left( (\rho_l u_l k) - \left( \mu_l + \frac{\mu_{l,tur}}{\sigma_k} \right) \nabla k \right) \right] = \alpha_l (G - \alpha_l \rho_l \varepsilon_l) \quad (13)$$

$$\frac{\partial}{\partial t}(\rho_l \alpha_l \varepsilon_l) + \nabla \cdot \left[ \alpha_l \left( (\rho_l u_l \varepsilon_l) - \left( \mu_l + \frac{\mu_{l,tur}}{\sigma_k} \right) \nabla \varepsilon_l \right) \right] = \alpha_l \frac{\varepsilon_l}{k} (C_{\varepsilon 1} G - C_{\varepsilon 2} \alpha_l \rho_l \varepsilon_l)$$

$$\mu_{l,tur} = C_{\mu} \rho_c \frac{k_c^2}{\varepsilon_c}$$

where  $C_{\varepsilon 1}, C_{\varepsilon 2}, C_{\mu}, \sigma_k, \sigma_\varepsilon$  are the standard k- $\varepsilon$  model constants and  $G$  is the turbulence production term. Therefore, the turbulent viscosity of the continuous phase is calculated by:

$$\mu_{\alpha,eff} = \mu_{\alpha,lam} + \frac{\mu_{\alpha,tur}}{\sigma_k} + \mu_s \quad (14)$$

where  $\mu_s$  is Sato's bubble-induced turbulent viscosity.

### 3.2. Shear Stress Transport Model

The k- $\varepsilon$  turbulence model often cannot predict the beginning and the amount of flow separation under adverse pressure gradient conditions. In general,  $\varepsilon$ -based turbulence models predict the onset of separation too late and under-predict the amount of separation later on. The more prominent two-equation models in this area are the based models of Menter [15-16]. The k- $\omega$  based Shear-Stress-Transport (SST) model was designed to give the highly accurate predictions of the beginning and the amount of flow separation by the inclusion of transport effects into the formulation of the eddy-viscosity:

$$\mu_{tur} = \frac{a.k}{\max(a\omega, SF)} \quad (15)$$

in this formulation,  $S$  is strain rate and  $F$  blending function.

The RNG k- $\varepsilon$  model, an alternative to the standard model, offers little improvement compared to the standard model by replacing a new RNG constant ( $C_{\varepsilon RNG}$ ) instead of conventional k- $\varepsilon$  constant ( $C_{\varepsilon}$ ).

### 4. Characteristics of Helical Coil

Fig.1 gives the schematic of a helical coil. The pipe has an inner diameter  $2R$  and the coil has a diameter of  $2R_c$ . The increase in elevation per revolution of pipe  $H = 2\pi p_s$  and  $p_s$  is pitch. The curvature and torsion of the helical coils are defined as follows [17]:

$$Curvature = \frac{R_c}{\left(R_c^2 + p_s^2\right)} \quad (16)$$

$$Torsion = \frac{p_s}{\left(R_c^2 + p_s^2\right)} \quad (17)$$

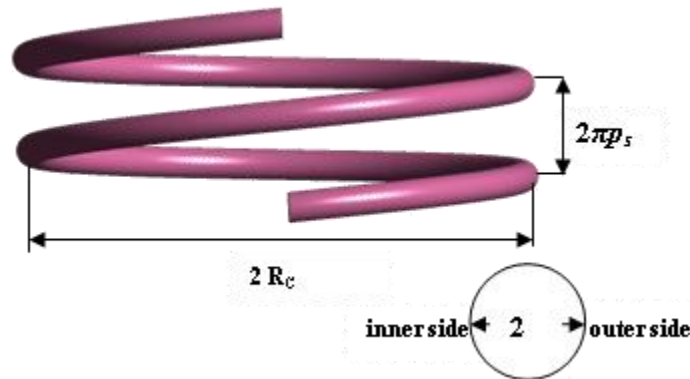


Fig. 1. The schematic of a helical coil.

As radius of curvature and pitch of a helical coil becomes infinity, the helical coil tends to a horizontal and vertical pipe, respectively. On the other hand, by reducing the radius of curvature the centrifugal forces acting on the fluid flow in helical coil increases.

### 5. Boundary Conditions and Solution Method

The following boundary conditions were used in this study. Superficial velocity ( $u = 2$  m/s) for each of the phases and volume fraction of air at the inlet was specified (air void fraction equal to 0.2) and isothermal system was considered. No-slip wall boundary conditions were applied at the pipe wall. At the outlet of the pipe, a pressure boundary condition was applied

(relative pressure equal to zero). The simulations were carried out as 3-D up-flow in helical coils based on the two-fluid Eulerian-Eulerian approach combined with Population Balance Model (PBM). The conservation equations were discretized using finite volume method and high resolution scheme was used for all equations. SIMPLEC algorithm was used for pressure-velocity coupling. Water was considered as the continuous phase, and air as the dispersed phase. The PBM model has been used to account for the non-uniform bubble size distribution in gas-liquid mixture. Five groups of bubbles were selected, minimum and maximum of the bubbles diameter are 0.06 and 0.14 mm, respectively. Convergence criterion used was  $1.0 \times 10^{-5}$  for all of the items. The helical coil geometry are meshed by unstructured tetrahedral and wedges meshes. After verifying the grid independency, the total number of element obtained is 1107849 elements and the mesh size 1.5 mm was used. In solver settings, fluid timescale control was used auto timescale. The effect of gravitational force is applied in this analysis.

## 6. Results and Discussion

To study the characteristics of upward air-water two-phase flow through the helical coils, 12 cases with different cases of curvature and torsion were produced defined in table. 1.

Table 1. The details of cases studies

Case No.	H, mm	$2R_c$ , mm	Torsion/ $m^{-1}$	Curvature/ $m^{-1}$
1-2-3	20,30,60	100	1.27-1.89-3.69	19.91-19.82-19.29
4-5-6	20,30,60	200	0.32-0.48-0.95	9.99-9.98-9.91
7-8-9	20,30,60	300	0.141-0.21-0.42	6.66-6.66-6.64
10-11-12	20,30,60	400	0.08-0.12-0.24	5.00-5.00-4.99

The pressure contours are presented in Fig. 2 High-pressure region lies close to the bottom side of the pipe wall, because of the weight of the water column. It is obvious, especially, until  $\theta = 45^\circ$  (the angle  $\theta$  is measured from the inlet of the helical coil). Then, the acceleration force acting on the fluid flow leads to creation of high-pressure zone at the outer side of the pipe wall. As the fluid flowing upward, however, the contribution of the column weight is diminished and this leads to the fact that high-pressure zone is fixed at the outer side of the pipe wall. The developed pressure gradient of case no. 3 at each cross section is more than cases 1 and 2. It is expected that for cases with low curvature (similar to the straight pipe with infinity of radius of curvature) the pressure at each cross section to be nearly uniform. The developed radial pressure gradient resulted in the air bubbles migration toward the low pressure region i.e. the inner side of the pipe wall.

For evaluating the effect of turbulence modeling, global value of pressure drop was chosen as a measuring scale. The obtained pressure drop from the two combined form of SST-MUSIG model, k- $\epsilon$  MUSIG model and RNG k- $\epsilon$  MUSIG model for some cases are presented in table. 2. The well-known experimental correlation recommended by Czop *et al.* [8, 18] is used for evaluations and validation of our CFD codes. The results indicate that obtained results from the SST-MUSIG combined model is the best and RNG k- $\epsilon$  MUSIG model is the worst. For flows with separation and recirculating regions, the RNG k- $\epsilon$  model along with the modified coefficients provides results which are less diffusive. Therefore, in the following the SST-MUSIG combined model was chosen to study the hydrodynamic characteristics of two-phase flow in helical coils.

Unlike the bent tubes (with zero pitch) which high-pressure region is exactly at the outer side of the pipe wall, in helically pipes (with non-zero pitch) the high-pressure region is close to the bottom corner of the outer side of the pipe wall. As can be seen in Fig. 3, zooming on the air volume fraction contour plot one can see that, firstly, the high water concentration zone is developed at the bottom of the helical wall pipe. Since the pressure gradient and the amount of pressure at high- pressure zone in each cross section of case number 3 is more than cases 1 and 2, one can expect that separation of the dispersed air in helical coils with high torsion are more than the others with the same curvature.

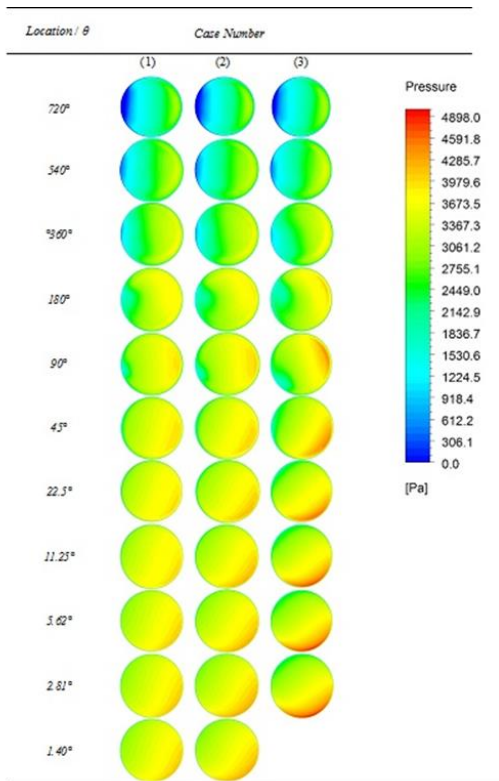


Fig. 2 Contour plots of pressure at different cross sections from SST-MUSIG model

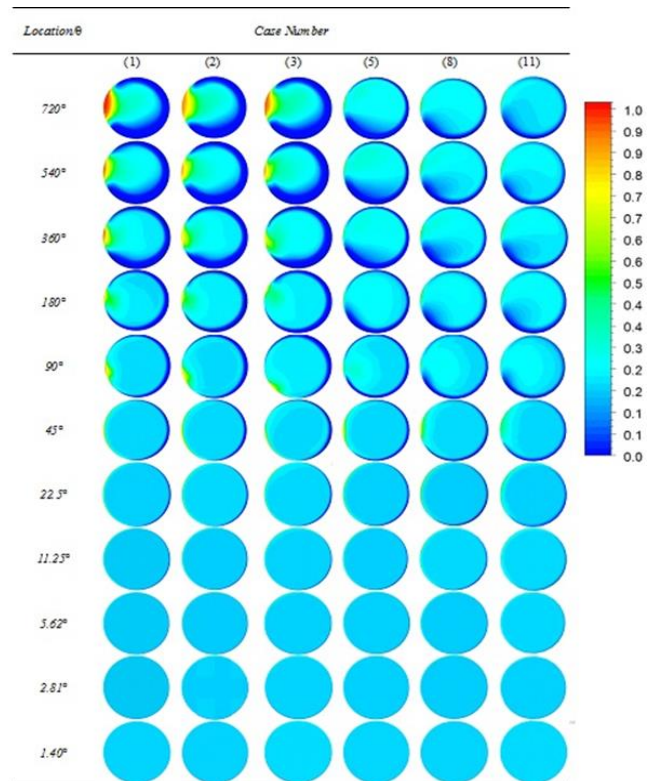


Fig. 3 The contour plots of air volume fraction at different cross sections from SST-MUSIG model

Table 2 The Average Absolute Deviation (AAD) for pressure drop results.

Case No.	AAD% for Pressure Drop		
	k-ε-MUSIG	RNGk-ε- MUSIG	SST - MUSIG
1	17.02	12.10	11.62
5	4.07	6.83	1.17
9	13.07	14.78	12.38
13	17.04	19.64	15.52
Total	12.80	13.34	10.17

For cases 1-3, the high concentration region of air is always near to the inner side of the pipe wall. It seems that occurrence of white eyes- regions have low pressure, high concentration of air and low velocity- in the cases with the higher radius of curvature is appeared sooner (in terms of  $\theta$ ) than cases with lower radius of curvature. In a similar manner to the rate of aggregation (fig. 3), the separation of the phases and appearance of the white eye depends on the stream-wise length, which acceleration forces affect the two-phase flow. However, the flow pattern of cases 5, 8 and 11, rather resemble a straight horizontal pipe. In this cases the acceleration forces acting on the fluid flow is lower than cases 1-3 and considerable volume of the separated air can rise toward the upper half of each cross section of the helical coil. It is also obvious from Fig. 4 that the pressure gradient of the cases with low radius of curvature is so high. In addition, for case no. 3 this value is more than cases 1 and 2.

According to Fig. 5, immediately, after pouring the two-phase flow in helical coil the coalescence of the particles leads to that the mean bubble diameter tends to remain approximately constant. At the same location (in terms of  $\theta$ ), the air-water two-phase flow through the helical coils of cases 10-12 experiences more stream-wise length ( $\theta.R_c$ ). In these cases, the rate of aggregation is more than other cases. However, the torsion has no measurable effect. Generally, two important reasons, which can influence the flow patterns of two-phase flow in helical coils, are geometry of the helical and the superficial velocity of the phases. Decreasing the water-air velocity ratio can convert the flow pattern from bubbly flow to plug and finally slug flow. Decreasing the radius of curvature and, consequently, increasing the secondary flow increases the collision of the bubbles and this may lead to the conversion of the flow pattern

from bubbly flow to plug flow [19]. However, the superficial velocity is more important. In these case studies, water-air velocity ratio that is equal to one is so much and therefore, in this level of velocity of the phases the flow pattern has no visible effect from the geometries and in all of the cases, aggregation of the bubbles produces the same mean bubble diameter (0.132 mm).

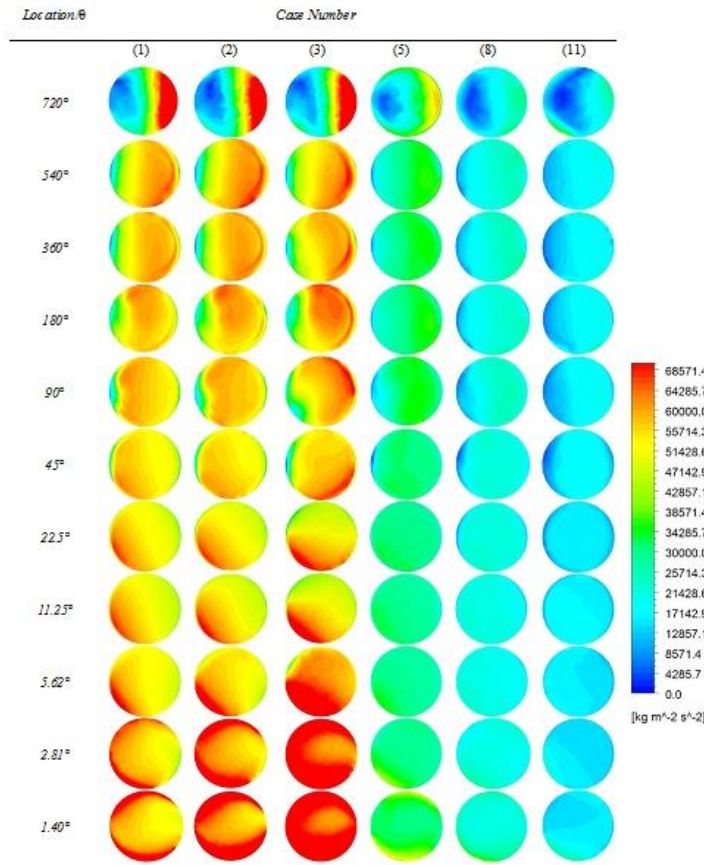


Fig. 4. The contour plots of pressure gradient.

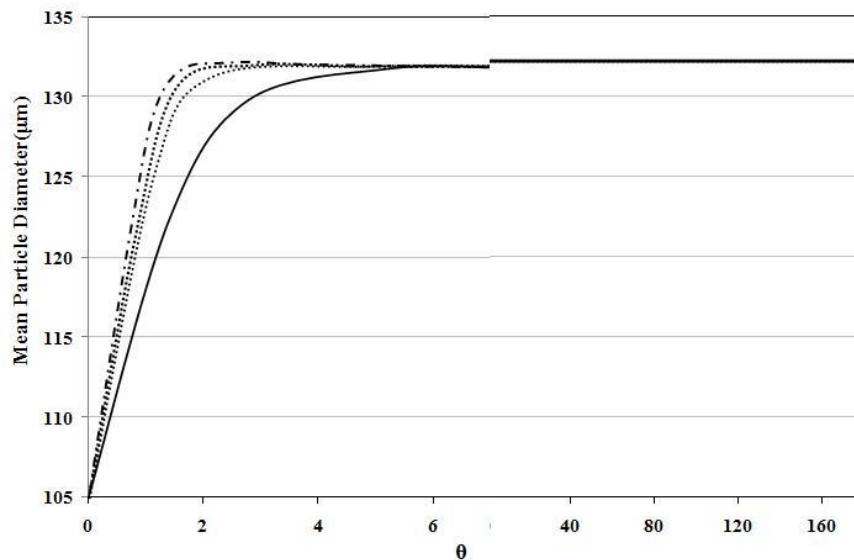


Fig. 5. Mean particle diameter of bubbles at different cross section from SST-MUSIG model; solid line (cases 1-3), circular dotted line (cases 4,5,6), square dotted line (cases 7,8,9), dashed line (cases 10,11,12).

Fig. 6 shows the contour plots of water velocity. In contrast to the flow in straight pipes, which their high velocity regions at each cross section form at the center of the pipe, the high velocity region in helical coils appears close to the outer side of the pipe wall. By acting the centrifugal forces on the fluid flow in the helical coil, immediately upon entering, the high velocity region lies adjacent to the bottom of the pipe wall. By flowing the fluid into the pipe, at location about  $\theta = 45^\circ$ , the high velocity region ascends and, finally, fixed at the outer side of the pipe wall. It seems that the onset of transition of high velocity region is delayed by increasing the curvature of the helical coils. The appearance of white eyes i.e. the low velocity zone at each cross section appears at  $\theta = 45^\circ - 90^\circ$ . The velocity gradient at each cross section of case no. 3, which has the higher torsion, is higher than other cases. It is also in according with the pressure contour plots of case no.3 (Fig. 2).

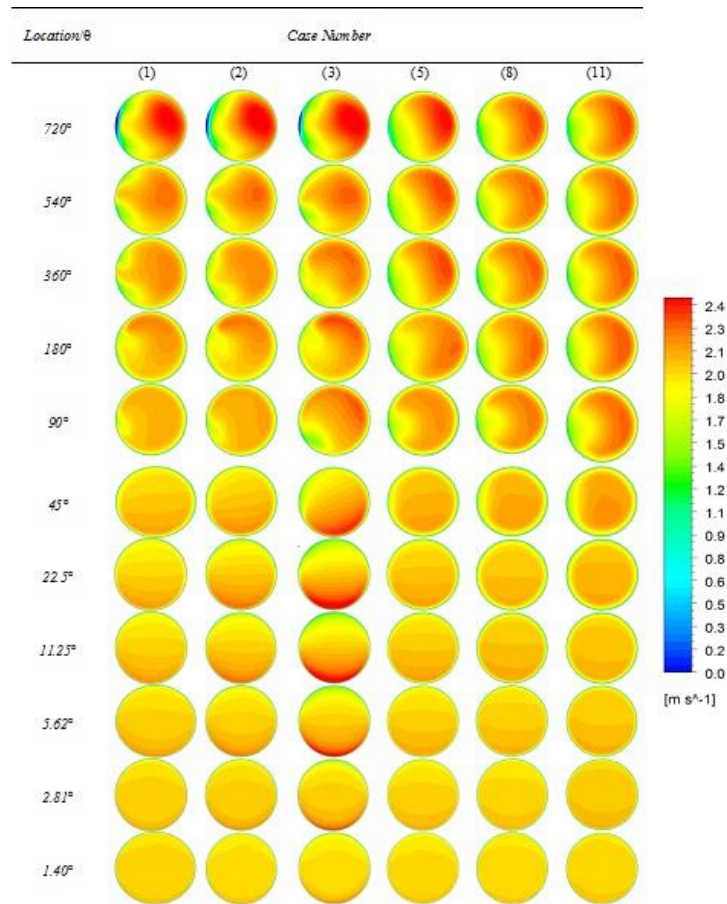


Fig. 6. The contour plots of water velocity at different cross sections from SST-MUSIG model.

The core part of the fluid at each cross section experiencing more centrifugal acceleration than that part close to the walls of a helical coil, repeatedly hits to the outer-side of the pipe and returns to the inner side of the pipe, introducing a secondary flow which is perpendicular to the main stream direction. The secondary motion of the fluid, however, is an important virtue of helical coils resulted in the use of helical coils as high-performance heat exchanger tools. The secondary motion, indeed, sweeps the heat exchanged by the fluids.

Our findings revealed that the secondary flow has two major effects on the flow pattern. One is that secondary flow encourages the bubbles to migrate from the inner side to the other side of the pipe wall (Fig. 3); however, the developed high-pressure zone by creating buoyancy strength inhibits freedom of the bubbles. The second, the secondary flow leads to the more collision of the bubbles resulting in aggregation. On the other hand, the developed pressure gradient fixes this situation and concentrates the bubbles at the inner side of the pipe wall. The authors think that for cases with the low density of dispersed phase, the role of the developed pressure gradient in separation of the phases is very important. The separation of the phases in cases 1 through 3 and especially case no. 3 are more than the other

cases (see Fig. 3). Generally, in two-phase fluid flow, by increasing the velocity of each phase, that phase tends to be continuous. For example, in plug two-phase flow, increasing the velocity of the gas, finally, introduces a slug flow pattern. Therefore, one can expect that because of the buoyancy component, at the same boundary condition, the flow pattern of a vertical straight tube in comparison with the horizontal tube has more chance to experience slug flow and in addition, in this situation the region on which two-phase flow can be bubbly flow is reduced. Hence, case no. 3, which more resembles a vertical tube (a helical coil with infinity of pitch), has more chance of collision and coalescence of the bubbles. Hence, separation of air in that case is considerably high.

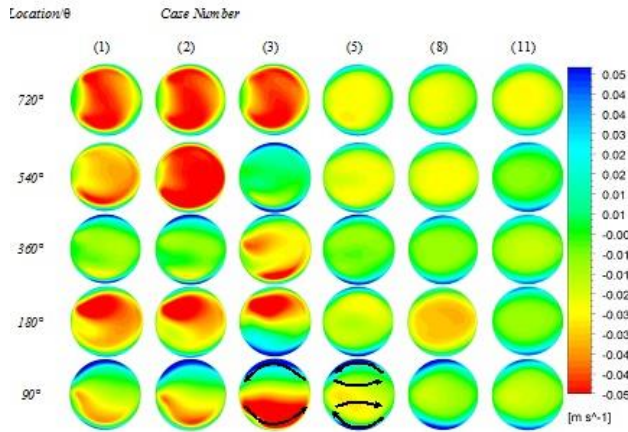


Fig. 7. The contour plots of water secondary flow from SST-MUSIG model.

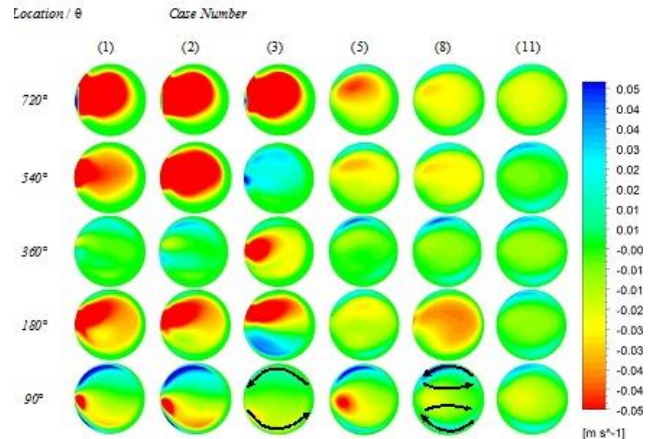


Fig. 8. The contour plots of air secondary flow from SST-MUSIG model.

Fig. 7 shows the secondary flow, flowing in direction perpendicular to the main stream of the helical coil. It reveals that, the magnitude of this motion in cases 1-3 is more than the other cases. In all of the cases, the existence of the secondary flow in the form of pair-recirculation zone is obvious. However, in case 3, which the pitch is enlarged, in the first contour plot the single-recirculation zone is developed. Buoyancy component of the dispersed air phase resulted in decreasing the magnitude of air secondary flow in comparison to the water secondary flow (Fig. 8).

## 7. Conclusions

The hydrodynamic characteristics of isothermal upward turbulent two-phase air-water flow in helical coils were investigated using computational fluid dynamics. Population Balance Modeling (PBM) approach was applied for size distribution developed due to coalescence and breakup of bubble groups.

The capability of proposed CFD-PBM model in combination with  $k-\epsilon$  and SST turbulence models was evaluated, in hydrodynamic calculation of helical coil, in combination with CFD-PBM model the SST turbulence model is more suitable than  $k-\epsilon$  turbulence model.

Immediately after pouring the two-phase flow of poly-dispersed air in water, the air bubbles are aggregated and concentrated to the inner side of the pipe wall. However, the mean diameter of the bubbles along the flow was nearly constant. The secondary flow influences two-phase fluid flow in helical coils, encourages the bubbles to aggregate, and develops radial pressure gradient leading to concentrate the air at the inner side of the pipe walls.

The beginning of creation of low pressure, high concentration of air and low velocity zone (white eyes) appears at location  $\theta = 45^\circ - 90^\circ$ . For improving heat transfer in high temperature heat exchanger tools, such as boilers, the purpose of using helical pipes instead of straight pipes, however, may be limited by the fact that the minimum capacity of heat transfer is attributed to the inner side of the pipe which is concentrated by air or vapor. Therefore, in high temperature heat exchanger devices, the orientation and low velocity of the air or vapor volume fraction in two phase flow maybe make a tube prone to the unexpected failure by overheating of the pipe wall [20]. However, it is strongly depended on some other parameters,

such as air volume fraction, pressure (in vapor-liquid two phase flow), pitch, flow pattern of hot gas (flue gas), velocity of liquid and dispersed gas phase, etc.

The results were shown that if the torsion of a helical coil is increased, the secondary flow from two recirculation structures becomes a single vortex pattern. The secondary flow has two major effects on flow pattern; one is the transition of bubbles toward the outside of the pipe wall and the other is collision and aggregation of the bubbles. The former and the later, however, is controlled and supported by developed pressure gradient, respectively.

## References

- [1] Abdalla, M.A., 1994, A four-region, moving-boundary model of a once through, helical-coil steam generator, *Ann. Nuc. Energy*. 21, 541–562.
- [2] Jayakumar, J.S., Grover, R.B., 2002, Response of a two-phase system subject to oscillations induced by the motion of its support structure, *Int Comm. Heat Mass Transfer*. 29, 519-530.
- [3] Karbasian, H.R., Kangarsgahi, A.F., 2013, Numerical simulation of the erosion in bend pipes caused by gas-particle flows, *Pet. Coal*. 55, 2, 128-132.
- [4] Jones, D.R.H., 2004, Creep failures of overheated boiler, superheater and reformer tubes, *Eng Fail Anal*. 11, 873–93.
- [5] Serizawa, A., Kataoka I., Phase distribution in two phase flow, *Proc. ICMHT Int. Seminar on Transient Phenomenon in Multiphase Flow*, Dubrovnik.
- [6] Mandhane, J.M., 1974, A flow pattern map for gas-liquid flow in horizontal pipes., *Int. J. Multiphase Flow*. 1, 537–553.
- [7] Kasturi, G., Stepanek, J.B., 1972, Pressure drop and void fraction measurements in cocurrent gas-liquid flow in a coil, *Chem. Eng. Sci*. 27, 1871–1880.
- [8] Czop, V., Barbier, D., Dong, S., 1994, Pressure drop, void fraction and shear stress measurements in an adiabatic two-phase flow in a coiled tube, *Nucl. Eng. Des*. 149, 323–333.
- [9] Prince, N.J., Blanch, H.W., 1990, Bubble coalescence and break-up in air sparged bubble columns, *AIChE J*. 36, 1485-1499.
- [10] Luo, H., Svendsen, H.F., 1996, Theoretical model for drop and bubble break-up in turbulent dispersions, *AIChE J*. 42, 1225–1233.
- [11] Jayakumara, J.S., Mahajani, S.M., Mandal, J.C., Iyer, K. N., Vijayan P.K., 2010, Thermal hydraulic characteristics of air-water two-phase flows in helical coils, *Che. Eng. Res. & Desi*. 88, 501–512.
- [12] Takamasa, T., Kondo, K., Measurement of bubble Motion in bend tube using image processing method, *ANS Proc. Of the Nat. Heat Transfer Conference, HTC-Vol.8*, pp.110-117, Oregon, USA, 5-9 August 1995.
- [13] Ishii, M., Zuber, N., 1979, Drag coefficient and relative velocity in bubbly, droplet or particulate flows, *AIChE J*. 25, 843–855.
- [14] Sato, Y., Sekoguchi, K., 1975, Liquid velocity distribution in two-phase bubble flow, *Int. J. Multiphase Flow*., 2, 79–95.
- [15] Menter, F.R., 1994, Two-equation eddy-viscosity turbulence models for engineering application, *AIAA-J.*, 32, 1598-1605.
- [16] Frank, T., Lecher, R., Menter, F., *Workshop on Two-Phase Flow Predictions*, Merseburg, Germany, 5-8 April 2005.
- [17] Hüttl, T.J., Fridrich, R., 2000, Influence of curvature and torsion on flow in helically coiled pipes, *Int. J. Heat & Fluid Flow*., 21, 345-353.
- [18] Jayakumara, J.S., Mahajani, S.M., Mandal J.C., Vijayan, P.K., Bhoi, R., 2008, Experimental and CFD estimation of heat transfer in helically coiled heat exchangers, *Chem. Eng. Res. & Des.*, 86, 221–232.
- [19] Murai, Y., Yoshikawa, S., Toda, S., Ishikawa, M., Yamamoto, F., 2006, Structure of air-water two-phase flow in helically coiled tubes, *Nucl. Eng.Des.*, 236, 94–106.
- [20] Abbasfard, H., Ghanbari, M., Ghasemi A., Ghader, S., Rafsanjani, H.H., Moradi, A., 2012, *Engineering Failure Analysis*, 26, 285–292.